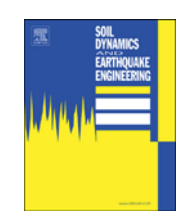
ELSEVIER

Contents lists available at ScienceDirect

# Soil Dynamics and Earthquake Engineering

journal homepage: www.elsevier.com/locate/soildyn



# A Site-specific ground-motion simulation model: Application for Vrancea earthquakes



Alin Radu<sup>a,\*</sup>, Mircea Grigoriu<sup>b</sup>

- <sup>a</sup> University of Bristol, Bristol, UK
- <sup>b</sup> Cornell University, Ithaca, NY, United States

#### ARTICLE INFO

Keywords:
Synthetic earthquakes
Site-specific
Non-stationary
Non-Gaussian
Ground-motion simulation
Earthquake engineering
Vrancea earthquakes
Limited data
Bayesian statistics

#### ABSTRACT

A large number of ground-motion time histories is required for a reliable probabilistic seismic-hazard analysis. However, insufficient ground-motion records has been a major issue in earthquake engineering even in high-seismicity areas. Stochastic and seismological ground-motion models are used to simulate time histories in order to overcome this issue. Many times these models require a large number of records for calibration, are available only for regions with a wealth of data, or fail to characterize well specific sites.

The current paper introduces a novel stochastic ground-motion model that allows simulation of realistic non-stationary, non-Gaussian time histories that are statistically consistent with data even at sites with very low numbers of records. This goal is achieved by combining the prior knowledge from a seismological model, calibrated to global data, with the site-specific data within a Bayesian framework. The proposed model uses the specific barrier model as the seismological model and numerical results consistent with records from a nuclear powerplant site in Romania are presented.

# 1. Introduction

Detailed seismic-risk assessment is a requirement for various applications, from the design of high-value structures to the development of risk-management solutions and risk-transfer solutions for the (re) insurance market. An accurate evaluation of the seismic risk of structures at specified sites requires the dynamic analyses of those buildings subjected to site-specific records. This is usually constrained by the limited number of recorded ground motions available at individual sites. The methods proposed to overcome this issue can be split in two classes: methods that select ground-motion records from large datasets, and scale them to desired intensity measures; and methods that simulate artificial ground-motion records.

A review of ground-motion selection is provided in [1]. A popular procedure is to select ground-motion records to match a response target-acceleration spectrum [2–4]. Computational methods for selecting ground motions and selection algorithms were developed in [5,6]. The selected records are then used for probabilistic seismic-hazard analyses by scaling them to obtain ground motions of various intensities. This procedure has limitations since it only changes the amplitude of the motion, but not its frequency content [7]. The alternative to scaling selected ground motions is the simulation of ground motions by using either stochastic models or seismological models. For the

purpose of this discussion, we define seismological models as the models whose calibration involves event characteristics of a physical nature, such as stress drop, rupture model, etc., while stochastic models are mathematical models calibrated just to recorded time histories and their description in terms of magnitude, epicentral distance, soil type, etc.

Seismological models, such as the point-source model SMSIM [8] or the finite-fault model EXSIM [9], used for ground-motion simulation show that important work has been developed in this area. Note that these two models are defined as stochastic in the seismological community [12]. Detailed comparisons between the two models have been presented in [10,11]. Usually seismological and physics-based models are very complex and target specific events, such as a hypothetical 7.8-magnitude event on the San Andreas fault in California [13]; the 1915 Marsica earthquake in Italy [14]; the 1999 7.1-magnitude earthquake in Turkey [15]; or the 2011 9.1-magnitude event in Japan [16,17]. A model in [18] is called "semi-stochastic", since it combines a physics-based model for the low-frequency and a stochastic model for the high-frequency contributions.

The stochastic models for ground-motion simulations represent more of an engineering approach which relies on the idea of earthquakes as filtered Gaussian noise with finite duration [19,20]. Stochastic models are usually defined as parametric models which can be

E-mail address: alin.radu@bristol.ac.uk (A. Radu).

<sup>\*</sup> Corresponding author.

fit to specified regions, such as north-western Europe in [22], or calibrated to generate ground motions compatible with design response spectra [21,23] or given ground-motion prediction equations [24]. However, models with a large number of parameters, such as [25-27], may be difficult to calibrate reliably in regions with poor ground-motion records. Others [28] postulate mathematical models, in this case the Karhunen-Loève expansion, to produce artificial records, by estimating the distributions and the second-order moment properties from recorded ground motions. Special attention has been given to the representation of the non-stationary character of the ground motions [29] in stochastic models. Many formulations of the evolutionary powerspectral density for ground-motion simulations [30-32] use the model introduced by Priestley [33]. Other models [25,34] use a frequency filter to achieve this goal, while in a newer approach [26,27] a multimodal Kanai-Tajimi spectrum is used to describe the time dependency of the frequency content. In Ref. [35,36] a spectral density estimated by wavelets is used to describe the evolution in time of the spectral values of simulated ground motions. In a more comprehensive context of utilizing wavelets, a recent paper [37] proposes the construction of a power-spectral density function for non-stationary processes based on a compressive-sensing approach, for the purpose of reconstructing stochastic processes with scarce or incomplete data. In a different approach [38], empirical ground-motion prediction models are used to produce realistic Fourier spectra for the ground-acceleration processes, whose non-stationary character is modelled by log-normal distributions of the P- and S- pulse arrivals.

The current study proposes a new stochastic model that can simulate site-specific ground motions statistically consistent with site data. The model proposed combines site records with a seismological model within a Bayesian framework in order to describe the frequency content of the motions, and assumes a non-Gaussian distribution for the motion in order to incorporate the contribution of site records to other statistical moments, besides the mean and variance. The importance of hazard-consistent ground motions has been addressed before in [39], and a recent study [40] shows the significant effects of soil amplifications on ground motions. The seismological model adopted as part of our development is the specific barrier model (SBM) [41], calibrated to regional data in [42]. An augmented version of the model with additional source characteristics is presented in [43,44]. The SBM describes the frequency content of ground motions as a function of magnitude, epicentral distance, seismological regime and soil type. Our paper is structured in three main parts: model description, model calibration, and model evaluation. In summary, our model is a zero-mean, non-Gaussian stochastic process with second-order moment properties defined by a parametric seismological-based, one-sided, power-spectral density. The non-stationary character of the motion is achieved using both amplitude- and frequency-modulation parametric functions. In the model-calibration part, the probability distributions of the frequencyrelated parameters are updated to the site records. In the final part, the model is evaluated by comparison with an independent regional ground-motion prediction model in terms of intensity distributions. Calibration and numerical examples shown in the paper are for the Cernavodă site of a nuclear power plant in Romania, which lacks a large number of records, but which would require an accurate seismic-hazard analysis in case of a disaster-risk-reduction study.

## 2. Ground-motion model

The analysis of real ground-motion records shows that they are samples x(t),  $0 \le t \le t_f$  with time length  $t_f$  of complex stochastic processes  $X(t; \Theta, \Psi)$ , which can be simplified in three natural distinct time-sections [45]: (1) a built-up part, in which amplitudes  $\max_{0 \le t \le t_f} \{x(t)\}$  increase with time until they reach their highest-intensity range, (2) a stationary part, in which amplitudes preserve their highest-intensity characteristics, and (3) a decaying part, in which amplitudes decay exponentially over time. Fig. 1 (a) shows this split for

a ground-motion record. A further analysis in the frequency domain of these three parts of the record shows that the frequency content of the three parts is significantly different, as seen in Fig. 1 (b). Thus, not only the ground-motion amplitudes are non-stationary but also their frequency content.

More techniques used to perform time-frequency analyses of nonstationary signals are shown in [46], or more recently in [47] by using a Hilber spectrum. Following the observations above, the ground-motion model proposed for the simulation of site-specific ground motions is a non-stationary stochastic process

$$X(t; \Theta, \Psi) = c(t)Y(h(t; \Psi); \Theta), 0 \le t \le t_f, \tag{1}$$

where  $t_f$  is the duration of the motion, and  $\Theta$  and  $\Psi$  are stochastic parameters calibrated to site records. Functions c(t) and  $h(t;\Psi)$  are the amplitude- and frequency-modulation functions. The process  $Y(t;\Theta)$  is a zero-mean, stationary process with second-order moment properties governed by the parametric one-sided power-spectral density function  $g_Y(\nu;\Theta)$ , with the random parameter  $\Theta$ . Function  $g_Y(\nu;\Theta)$  is an updated version of the one-sided power-spectral density function  $g_{SBM}(\nu)$  provided by the specific-barrier model (SBM) [41,42]. The SBM is a seismological model calibrated to global data, and provides as an output the function  $g_{SBM}(\nu)$ , as a function of the moment magnitude m, epicentral distance r, type of soil and seismic regime. Note that for simplification purposes, the notation regarding these parameters is not used in the remainder of the paper. The random vector  $\Theta$  in  $g_Y(\nu;\Theta)$  is used to update  $g_{SBM}(\nu)$  to site records, as shown previously in [48], a methodology which is described in the next section.

A gamma model [31] is used for the amplitude-modulation function:

$$c(t) = \alpha t^{\beta} \exp\left\{-\gamma t\right\}, \ 0 \le t \le t_f, \tag{2}$$

where  $t_f$ ,  $\alpha$ ,  $\beta$  and  $\gamma$  are also outputs of the SBM, and are deterministic functions of (m, r), soil class, and seismic regime. Note that these parameters could be randomized, too, but our model calculates site-specific probability distributions only for the parameters affecting the frequency content of the motions for two reasons: (1) the response of structures is highly sensitive to the frequency content of the input, and (2) a large number of random parameters would limit the usefulness of the model in regions with little data.

A power-spectral density model which uses a positive, real-valued, increasing frequency-modulation function  $h(t; \Psi)$ , with zero slope at t=0, to describe the time evolution of the frequency content is adopted [30]. A log-normal parametric model is considered for  $h(t; \Psi)$ :

$$h(t; \Psi) = \frac{1}{\Psi_2 \sqrt{2\pi}} \int_0^t u^{-1} \exp\left(\frac{-(\ln(u) - \Psi_1)^2}{2\Psi_2^2}\right) du,$$
(3)

where  $\Psi$  is a random vector with coordinates  $[\Psi_1, \Psi_2]$ . The log-normal cumulative function was chosen because besides the fact that it fulfils all the requirements for  $h(t; \Psi)$ , it also covers a large range of possibilities with just two parameters, which control both the position of the function on the t axis as well as the function's shape. Finally, we can conclude that the process  $X(t; \Theta, \Psi)$  is obtained from the stationary process  $Y(t; \Theta)$  by (1) scaling its amplitudes to c(t), and (2) associating its scaled amplitudes to time-dependent frequencies.

A Gaussian distribution for the ground-motion process  $X(t;\Theta,\Psi)$  is the common assumption in previous studies [21,31,34]. However, the analysis of the ground-motion records in the PEER NGA-West dataset suggests that a normal distribution may not be appropriate. Fig. 2 shows the kurtosis  $\kappa$  calculated for all records in the dataset in comparison with the value  $\kappa=3$ , characteristic for Gaussian processes. The kurtosis in the data is most of the time well above 3 which suggests a limited usefulness of the Gaussian assumption. High kurtosis indicates heavy tails of the ground-motion distributions, and therefore higher peaks [49,50]. Hence, a non-Gaussian process with marginal distribution  $F_Y(y) = \mathbb{P}(Y(t;\Theta) \leq y), \forall 0 \leq t \leq t_f$  must be chosen for process

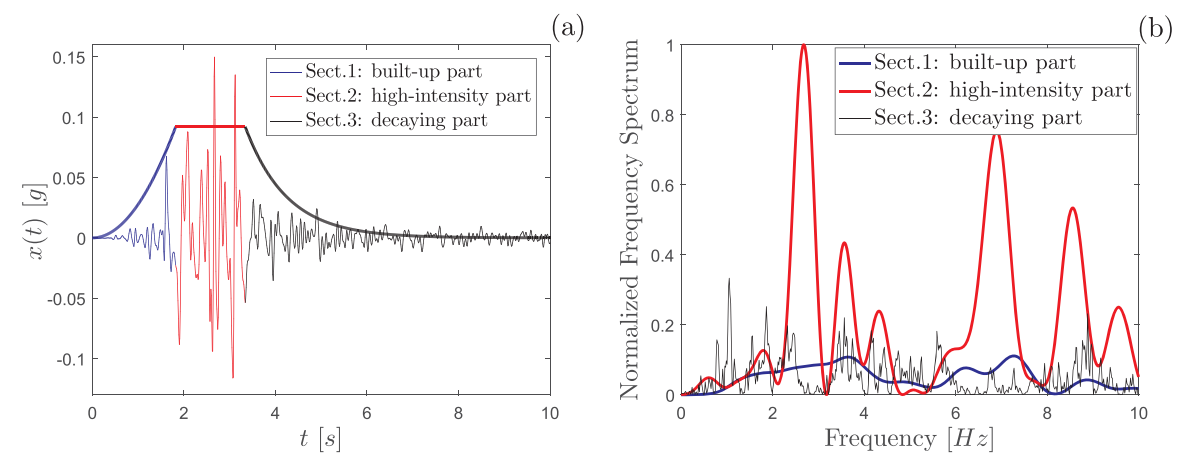


Fig. 1. Time dependency of (a) ground-motion amplitudes and (b) frequencies.

 $Y(t;\Theta)$ . We assume that the process  $Y(t;\Theta)$  follows a Student's T distribution with mean  $\mu$ , variance  $\xi\sigma^2/(\xi-2)$  and  $\xi$  degrees of freedom, and probability-density function

$$f_{Y}(y) = \frac{\Gamma(\frac{\xi+1}{2})}{\Gamma(\frac{\xi}{2})\sigma\sqrt{\pi\xi}} \left(1 + \frac{1}{\xi} \left(\frac{y-\mu}{\sigma}\right)^{2}\right)^{-\frac{\xi+1}{2}}.$$
(4)

The Student's T distribution suffices for the calibration of ground motions, because (1) it is symmetric about 0; (2) it is characterized by three parameters, which can accommodate the model's calibration to both the second-moment properties and the kurtosis; and (3) it has heavier tails than the Gaussian distribution. The kurtosis for the Student's T distribution of process  $Y(t; \Theta)$  is only a function of the number of degrees of freedom  $\kappa = 6/(\xi - 4)$ , for  $\xi > 4$ . Parameter  $\xi$  is calibrated for the NGA-West dataset shown in Fig. 2 (a), since the soil type at a site is assumed to be constant. The SBM supports soil classification provided by the National Earthquake Hazards Reduction Program (NEHRP). Thus, the kurtosis values for the records in the NGA-West dataset are grouped into the five NEHRP classes by their shearwave velocities  $v_{s30}$ , and mean values for the kurtosis  $\kappa$  and parameter  $\xi$ for the distribution  $F_Y(y)$  are provided in Table 1. Fig. 2 (b) shows the skewness for the same dataset. The skewness values  $\varsigma$  are unbiased around zero value, which support our choice of a symmetrical distribution for the ground-motion process X(t).

Fig. 3 also shows the kurtosis for the data points in the NGA-West dataset grouped in the NEHRP soil classes. Even though the mean parameter  $\xi$  looks similar between NEHRP soil classes, the log-normal

**Table 1** Average kurtosis  $\kappa$  and degrees of freedom  $\xi$  calibrated to NEHRP Soil-Classification.

NEHRP Class	Description	Average $v_{s30}[m/s]$	κ	ξ
A	Hard rock	$v_{s30} > 1500$	21.3	4.3
В	Generic rock	$1500 \ge v_{s30} > 760$	14.4	4.4
С	Very dense soil	$760 \ge v_{s30} > 360$	14.3	4.4
D	Stiff soil	$360 \ge v_{s30} > 180$	13.1	4.5
E	Soft soil	$180 \ge v_{s30}$	11.3	4.5

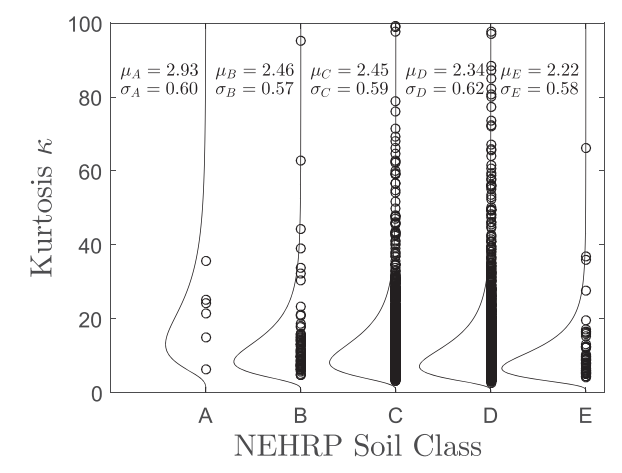
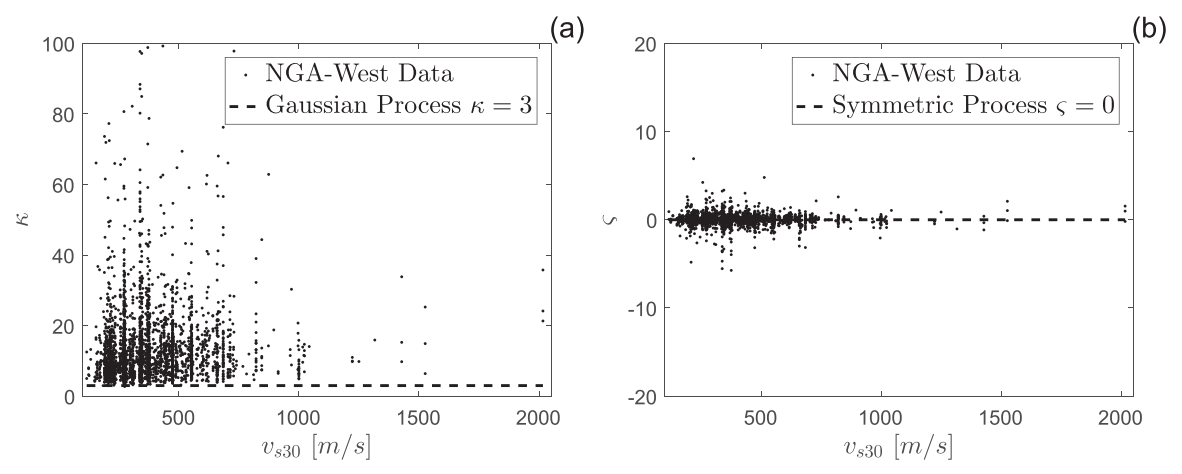


Fig. 3. Kurtosis of the ground-motion records in the NGA-West Dataset.



**Fig. 2.** (a) Kurtosis  $\kappa$  and (b) skewness  $\varsigma$  of the ground-motion records in the NGA-West Dataset.

distributions fitted to the kurtosis for each soil class, shown in Fig. 3, show that their distributions can be quite different. Maximum-like-lihood estimates of the mean and standard deviation for the kurtosis distributions are also provided, and this allows for simulation of  $\kappa$  values and therefore accounts for the variability in the distribution  $F_Y(y)$ .

Process  $Y(t; \Theta)$  can be calculated by using a monotonic memoryless-transformation model [51,52].

$$Y(t;\Theta) = F_Y^{-1} \circ \Phi(Z(t;\Theta))$$
 (5)

where (1)  $\Phi(x) = \int_{-\infty}^{x} \phi(y) dy$  is the standard Gaussian cumulative distribution function, with the probability density  $\phi(x) = (\sqrt{2\pi})^{-1} \exp\{-x^2/2\}$ , and (2)  $Z(t;\Theta)$  is a zero-mean, unit-variance, stationary Gaussian process with spectral density function  $g_Y(\nu;\Theta)/\int_0^\infty g_Y(\nu;\Theta) d\nu$ . The approximation that the spectral density of  $Z(t;\Theta)$  is just a scaled version of  $g_Y(\nu;\Theta)$  is based on the observation that the differences between the correlation in the non-Gaussian space and its correspondent in the Gaussian space are not significant for a broad range of values [52]. Note that the process  $Z(t;\Theta)$  also depends on (m,r), soil type and seismic regime.

In order to emphasize the importance of the non-Gaussian character of the ground-motion model, let  $Z(t;\Theta)$  be the Gaussian image of  $Y(t;\Theta)$  with the same second-order moment properties given by the spectral-density function  $g_{SBM}(\nu)$ . Even though the processes  $Y(t;\Theta)$  and  $Z(t;\Theta)$  have the same first two moments, they can have other very different properties when considering a value of kurtosis  $\kappa=4.5$ . Fig. 4 (a) shows a sample of  $Y(t;\Theta)$  and its correspondent in the Gaussian space  $Z(t;\Theta)$  for  $(m,r)=(5.8,50\,km)$ . Higher peaks are present in the sample of  $Y(t;\Theta)$ , which is consistent with the tail distributions of  $Y(t;\Theta)$  and  $Z(t;\Theta)$  shown in Fig. 4 (b). The mean crossing rates  $\eta_Y(z)$  and  $\eta_Z(z)$  at which processes  $|Y(t;\Theta)|$  and  $|Z(t;\Theta)|$  exceed a critical value z>0, respectively [53](Section 7.3) can be calculated analytically by

$$\eta_Y(z) = \frac{\dot{\sigma}}{2\pi\sigma} \exp\left\{-\frac{1}{2} \left[\Phi^{-1} \circ F_Y(z)\right]\right\} \tag{6}$$

$$\eta_Z(z) = 2 \frac{\dot{\sigma}}{\sigma \sqrt{2\pi}} \phi \left(\frac{z}{\sigma}\right),$$
(7)

where  $\sigma^2 = \int_{\nu \geq 0} g_{SBM}(\nu) d\nu$  and  $\dot{\sigma}^2 = \int_{\nu \geq 0} \nu^2 g_{SBM}(\nu) d\nu$  are the variances for processes  $Z(t;\Theta)$  and  $dZ(t;\Theta)/dt$ .

Fig. 5 shows the differences between the mean crossing rates  $\eta_Y(z)$  and  $\eta_Z(z)$  for processes  $Y(t;\Theta)$  and  $Z(t;\Theta)$ , respectively. The mean crossing rates of process  $Y(t;\Theta)$  are higher, which is consistent with the higher peaks present in its samples, as seen in Fig. 4 (a).

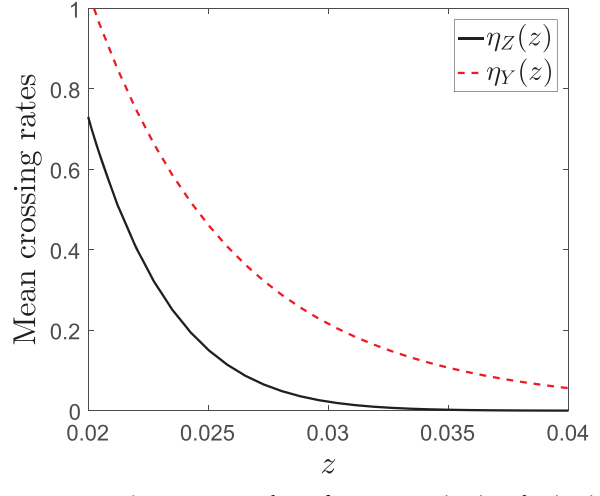


**Fig. 5.** Mean crossing rates  $\eta_Y$  and  $\eta_Z$  of processes  $Y(t;\Theta)$  and  $Z(t;\Theta)$ , respectively, for (m,r)=(5.8,50~km).

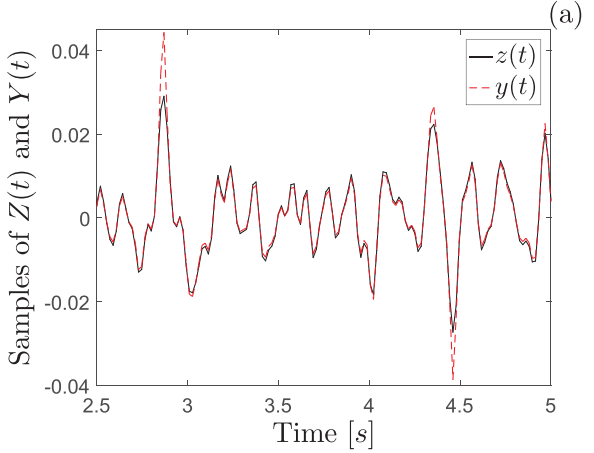
#### 3. Model calibration

The goal of the model is to provide site-specific ground motions statistically consistent with the recorded ground motions. In this section, stochastic parameters  $\Theta$  and  $\Psi$  for the power-spectral density function  $g_Y(\nu;\Theta)$  and the frequency-modulation function  $h(t;\Psi)$ , respectively, are calibrated to site records within a Bayesian framework.

#### 3.1. Site records: Cernavodă site in Romania

The ground-motion model in Eq. (1), presented in the previous section, can be calibrated for sites with a small number of records. For the numerical example in this section, earthquake records for the Cernavodă site in Romania are used. Romania is in a highly seismic region of Eastern Europe, which can produce deep, high-magnitude earthquakes with epicenters in the Vrancea region [54], but only a few records are available. The site chosen is of particular interest, since it hosts a nuclear power plant, and significant earthquake damage could have a major impact in the region. Only five two-horizontal component records are available at the site for earthquakes with moment magnitude higher than 5. Fig. 6 shows the ten records available at the site that will be used for the model calibration.

The records are available in the European Strong-Motion Database [55,56]. A brief summary of the five records used for calibration is provided in Table 2, including the date, moment magnitude and



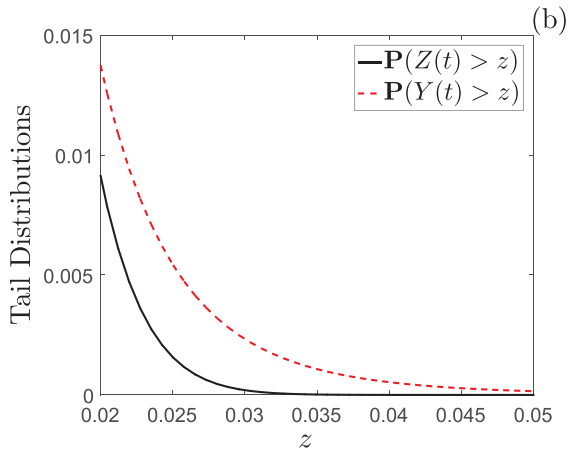


Fig. 4. (a) Comparison between a sample y(t) of  $Y(t; \Theta)$  and its Gaussian image  $Z(t; \Theta)$ , (b) Marginal distribution functions for processes  $Y(t; \Theta)$  and its Gaussian image  $Z(t; \Theta)$ .

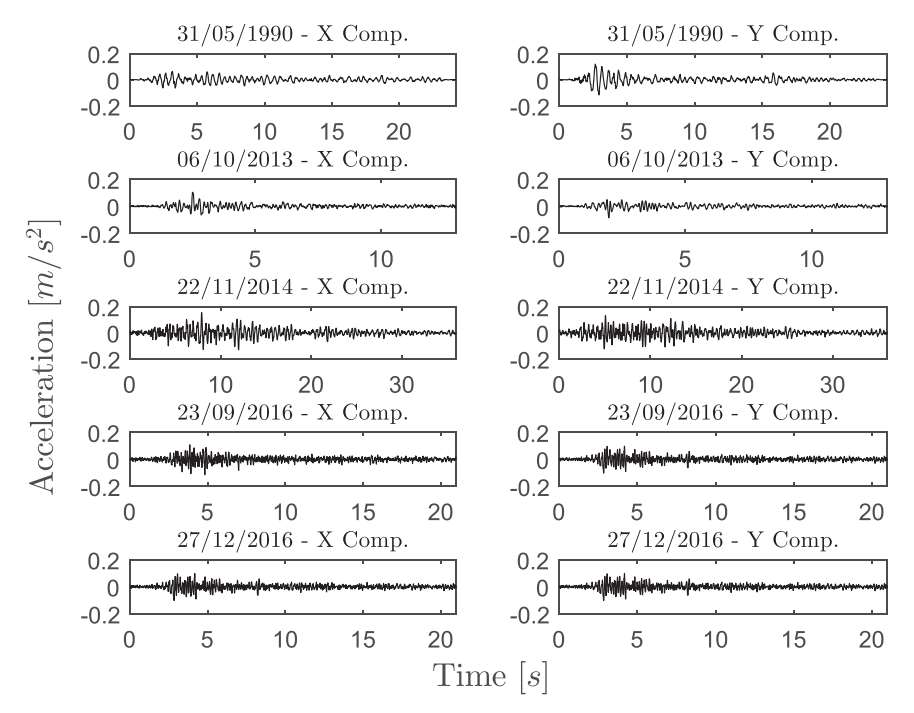


Fig. 6. Horizontal components for five earthquake records at the Cernavodă site in Romania.

 Table 2

 Summary of five earthquakes in Romania used for model calibration.

Date	Moment magnitude m	Epicentral distance $r[km]$
31/05/1990	6.3	194
06/10/2013	5.3	182
22/11/2014	5.6	187
23/09/2016	5.6	196
27/12/2016	5.6	191

epicentral distance.

The seismic design codes in Romania do not provide a classification of sites based on the shear-wave velocity  $v_{s30}$ , but only maps with design corner-periods  $T_c$ , which include the soil contribution to the seismic risk. A corner period  $T_c = 0.7 \, s$  from the Romanian seismic design code for Cernavodă [57] and a regression relation between  $v_{s30}$  and  $T_c$ , developed for different sites in Bucharest [58], would lead to a conclusion that Cernavodă is located on soft soil. In a separate study [59] it is shown that the nuclear power plant is, however, located on a layer of hard rock and therefore soil type A is used in the model calibration.

# 3.2. Bayesian updating

Stochastic parameters  $\Theta$  and  $\Psi$  are calibrated to site records combined with prior information about the model within a Bayesian framework. In this study, the prior information is reflected in the SBM, which can be substituted by any other seismological model that provides information on the ground-motion frequency content [17]. Note that the site records  $\widetilde{X}=\{\widetilde{x}_k(t_i),\ k=1,\ ...,N,\ i=1,\ ...,n\}$  used for the update are available in discrete form, i.e. as values at times  $t_i=i\delta t,\ i=1,\ ...,n$  at constant time intervals  $\delta t,$  where  $n=t_f/\delta t.$  The Gaussian images  $\widetilde{Z}=\{\widetilde{z}_k(t_i),\ k=1,\ ...,N,\ i=1,\ ...,n\}$  of records  $\widetilde{X}$  are calculated using the transformation suggested in Eq. (5), i.e.  $\widetilde{z}_k(t_i)=\Phi^{-1}{}_{^0}F_Y(\widetilde{x}_k(t_i)).$  Parameters  $(\mu,\sigma,\xi)$  of the Student's T distribution  $F_Y(y)$  are estimated from the mean, variance and kurtosis of the strong-motion part of each sample  $\widetilde{z}_k(t)$ , and are assumed to be time-invariant.

Bayes' theorem states that the posterior probability-density function

$$p(\theta, \psi | \widetilde{Z})$$
 of the unknown parameters  $\Theta$  and  $\Psi$  is 
$$p(\theta, \psi | \widetilde{Z}) \propto f(\theta, \psi) l(\widetilde{Z} | \theta, \psi), \tag{8}$$

where  $f(\theta, \psi)$  is a postulated prior density for  $\Theta$  and  $\Psi$  and  $l(\widetilde{Z}|\theta, \psi)$  is the likelihood function, which accounts for the significance of the observed data  $\widetilde{Z}$  in the distribution of  $\Theta$  and  $\Psi$ . A uniform prior probability-density function  $f(\theta, \psi)$  is used for  $\Theta$ .

For a given site, the update of the model is done for each set of (m,r), by writing the likelihood function  $l(\tilde{z}_k|\theta;\psi)$  for all  $N_{(m,r)}$  records  $\tilde{z}_k$ ,  $k=1,\ldots,N_{(m,r)}$  with a similar pair of parameters (m,r). Note that, for computational convenience, the update is done for moment magnitudes m and epicentral distances grouped in bins of size 0.1 and 5 km, respectively. The logarithmic form of the likelihood function, under the assumptions described previously, is written as:

$$\log(l(\tilde{z}_k|\theta;\psi)) \propto -\frac{n}{2}\log(|\Sigma(\theta,\psi)|) - \frac{1}{2}\sum_{i=1}^n (\tilde{\mathbf{z}}_k)^T \Sigma(\theta,\psi)^{-1} \tilde{\mathbf{z}}_k, \tag{9}$$

where  $|\Sigma(\theta, \psi)|$  is the determinant of the covariance matrix  $\Sigma(\theta, \psi)$  and  $\widetilde{\mathbf{z}}_k = \{\widetilde{z}_k(t_i)i = 1, ..., n\}$  denotes the vector with the discrete values of  $\widetilde{z}_k(t)$ . Note that the total number of records at a site  $N = \sum_{(m,r)} N_{(m,r)}$ . The components of the covariance matrix  $\Sigma(\theta, \psi) = \{\Sigma(t_u, t_v; \theta, \psi), u, v = 1, ..., n\}$  are calculated using the inverse Fourier transform of the power-spectral density function  $g_X(\nu; \Theta; \Psi)$  of process  $X(t; \Theta; \Psi)$  [60] (Section 3.6), which can be written as:

$$\Sigma(t_u, t_v; \theta, \psi) = c(t_u)c(t_v) \int_{\nu \ge 0} g_Y(\nu; \theta) \cos(\nu(h(t_u; \psi) - h(t_v; \psi))) d\nu,$$
(10)

where c(t) and  $h(t;\psi)$  are the amplitude- and the frequency-modulation functions shown in Eqs. (2) and (3), respectively. The power-spectral density  $g_Y(v;\Theta)$  can be seen as a stochastic version of the SBM  $g_{SBM}(v)$  and is defined as

$$g_{Y}(\nu;\Theta) = \sum_{i=1}^{3} \Theta_{i} \varphi_{i}(\nu), \tag{11}$$

where  $\Theta = [\Theta_i, i = 1, 2, 3]$  is a random vector and  $\varphi_i(\nu)$ , i = 1, 2, 3 are three functions of frequency  $\nu$  such that  $g_{SBM}(\nu) = \sum_{i=1}^3 \phi_i(\nu)$ , and therefore they depend on (m, r), soil type and seismic regime. The SBM

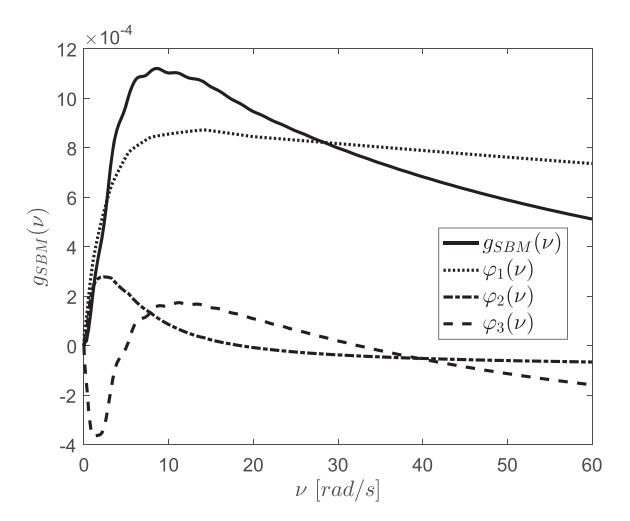


**Fig. 7.** Power-spectral density function  $g_{SBM}(\nu)$  and its components  $\varphi_i(\nu)$ ,  $i=1,\,2,\,3$ , for  $(m,\,r)=(6.3,\,195\,km)$ , soil type D and far-field seismic regime.

is only available in algorithmic form, therefore  $g_{SBM}(\nu)$  does not have a closed form. Functions  $\varphi_i(\nu)$ , i=1,2,3 can be obtained using a singular-value decomposition of functions  $g_{SBM}(\nu)$  for a given range of (m,r), frequencies  $\nu$ , soil type and seismic regime. A detailed description of the surrogate model and its statistical update using the strong-motion part of the records under the stationarity assumption is available in [48]. Fig. 7 shows the power-spectral density function  $g_{SBM}(\nu)$  and its components  $\varphi_i(\nu)$ , i=1,2,3, for  $(m,r)=(6.3,195\,km)$ , soil type D and far-field seismic regime. Note that individual components do not have any physical meaning, and, hence, them alone not representing power spectral-density functions,  $\varphi_i(\nu)$ , i=1,2,3 can take negative values.

Following the procedure described above, the distribution of the stochastic-model parameters  $[\Theta, \Psi]$  is updated in light of the observed data  $\widetilde{Z}$  at the Cernavodă station, and the corresponding posterior distribution  $p(\theta, \psi | \widetilde{Z})$  can be calculated.

Fig. 8 shows the marginal-probability densities of the  $\Theta$  components, i.e.  $p(\theta_1 | \widetilde{Z})$ ,  $p(\theta_2 | \widetilde{Z})$  and  $p(\theta_3 | \widetilde{Z})$ , respectively. Due to the limited number of records available at the site, no large deviations from the uniform prior distributions of  $\Theta_2$  and  $\Theta_3$  are noticed, a result consistent with [48], in which was shown both analytically and numerically, that the model converges to the "true" power-spectral density as the number of samples in the update increases.

Fig. 9 (a) and (b) show the two-dimensional marginal distribution  $p(\psi_1,\,\psi_2|\widetilde{Z})$  of  $\Psi=[\Psi_1,\,\Psi_2]$  and its projection, indicating the maximum likelihood estimator  $\widehat{\psi}_{MLE}=[1.5,\,0.81]$  of  $\Psi$  by a red marker. Similar to the previous statement, the posterior distribution of  $\Psi_2$  stays almost uniform, similar to its prior distribution, due to the limited number of records used for the update. For a better understanding of the effects of

the updates, plots of the updated power-spectral density functions are shown in Figs. 10 and 11. Fig. 10 (a) shows the mean and 95% confidence intervals (C.I.) for the power-spectral density function  $g_Y(\nu;\Theta)$ , and the prior and posterior densities of  $\Theta$ , for  $(m,r)=(6.3,195\,km)$ , soil type D and far-field seismic regime. No significant difference is noticed between the prior and the posterior C.I.s, but significant changes are observed from the prior to the posterior distribution of  $g_Y(\nu;\Theta)$  at a fixed frequency  $\nu=10\,rad/s$  in Fig. 10 (b).

The effects of the parameter  $\Psi$  are shown in Fig. 11 (a), in which the evolutionary power-spectral density function  $g_X$   $(\nu, t|\Theta=[1, 1, 1], \Psi=\widehat{\psi}_{MLE})$  is shown for  $(m, r)=(6.3, 195\ km)$ , soil type A and far-field seismic regime, for the maximum likelihood estimator  $\widehat{\psi}_{MLE}$  of  $\Psi$ . Note that  $\Theta=[1, 1, 1]$  corresponds to the SBM power-spectral density. In addition, Fig. 11 (b) shows the correlation functions  $\rho(\tau, t_0|\Theta=[1, 1, 1], \Psi=\widehat{\psi}_{MLE})$  at fixed times  $t_0\in\{3, 6, 10\}$  seconds and the corresponding  $g_{SBM}(\nu)$  for the same seismological parameters indicated above. The correlation function  $\rho(\tau, t_0|\Theta=[1, 1, 1], \Psi=\widehat{\psi}_{MLE})$  and the corresponding one-sided power-spectral density functions  $g_X(\nu, t_0|\Theta=[1, 1, 1], \Psi=\widehat{\psi}_{MLE})$  at fixed times  $t_0$  are Fourier pairs for fixed parameters  $\Theta$  and  $\Psi$ .

# 4. Model evaluation

Once the model parameters  $[\Theta,\Psi]$  have been statistically calibrated to site records,  $X(t|\Theta,\Psi)$  can be used to simulate site-specific ground-motion records for given seismological parameters. In order to evaluate the performance of the model, this section provides a summary of the model in the form of a sample-simulation algorithm and a qualitative comparison with another model in the region.

### 4.1. Simulation algorithm

A step-by-step algorithm for simulating a sample  $x_i(t|\theta_i,\psi_i)$  of  $X(t|\Theta,\Psi)$ .

- 1. Simulate a sample  $[\theta_i, \psi_i]$  of  $[\Theta, \Psi]$  from the posterior distribution  $p(\theta, \psi|\widetilde{Z})$  from Eq. (8);
- 2. For a fixed time step  $\delta t$  and a fixed frequency step  $\delta \nu$ , calculate  $g_Y(\nu_j, t_k; \theta_i; \psi_j)$  at each discrete time  $t_k = k \delta t$  and frequency  $\nu_i = j \delta \nu$ ;
- 3. Calculate the Gaussian process sample  $z_i(t_k)$  using the spectral representation [29] with the power-spectral density function  $g_Y(\nu_j, t_k; \theta_i; \psi_i)$ ;
- 4. Calculate the mean  $\mu$  and the standard deviation  $\sigma$  from  $g_Y(\nu_i, t_k; \theta_i; \psi_i)$  at each time  $t_k$ .
- 5. Simulate a value of the kurtosis  $\kappa_i$  from the distributions in Fig. 3 and calculate the degrees of freedom  $\xi_i$  for the Student's T distribution in Eq. (4).
- 6. Calculate the non-Gaussian image  $y_i(t_k)$  of  $z_i(t_k)$  at each time  $t_k$  from Eq. (5).
- 7. Scale amplitudes of  $y_i(t_k)$  using the function in Eq. (2) to calculate

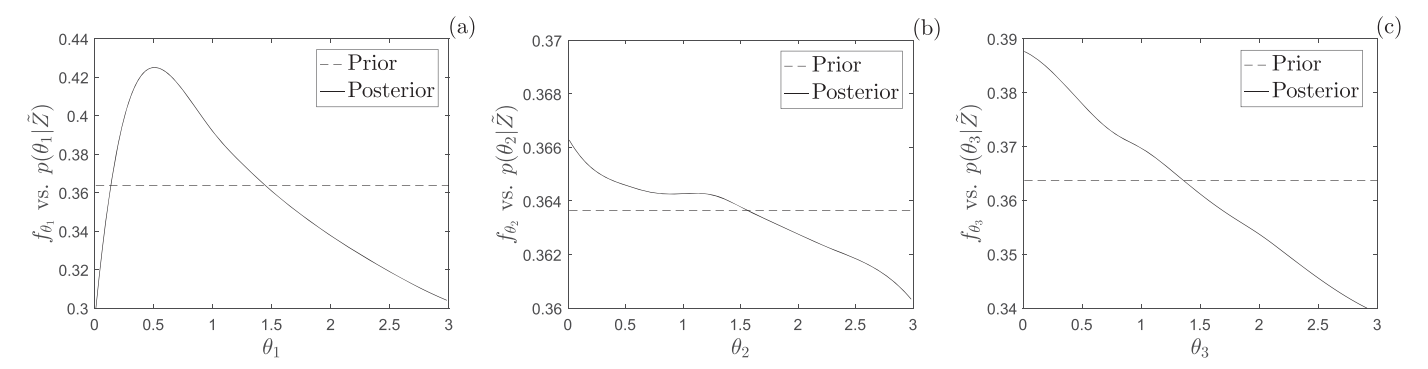


**Fig. 8.** Marginal distributions of the  $\Theta$  components: (a)  $p(\theta_1|\widetilde{Z})$ , (b)  $p(\theta_2|\widetilde{Z})$ , (c)  $p(\theta_3|\widetilde{Z})$ .

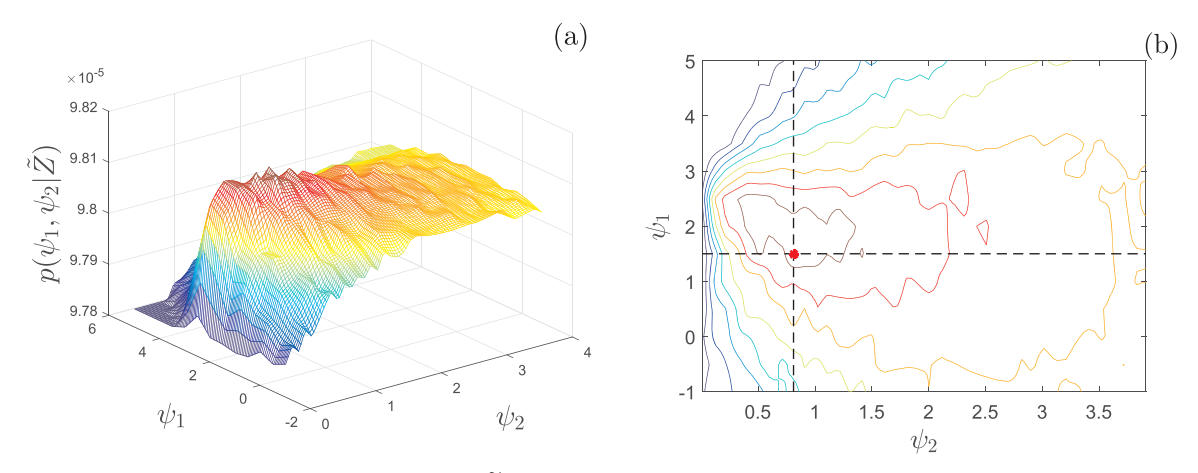
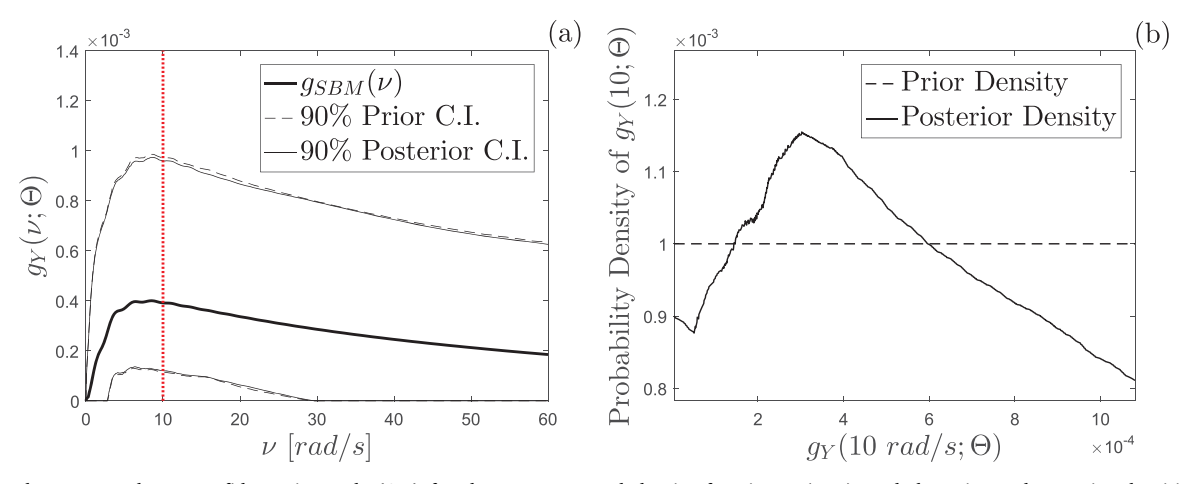


Fig. 9. (a) Marginal distribution of the  $\Psi$  parameter  $p(\psi_1, \psi_2 | \widetilde{Z})$ ; and (b) its projection, indicating the maximum likelihood estimator of  $\Psi$  in red star.



**Fig. 10.** (a) The mean and 95% confidence intervals (C.I.) for the power-spectral density function  $g_Y(\nu;\Theta)$ , and the prior and posterior densities of  $\Theta$ , for  $(m,r)=(6.3,195\ km)$ , soil type A and far-field seismic regime; (b) The prior and posterior distributions of  $g_Y(\nu;\Theta)$  at a fixed frequency  $\nu=10\ rad/s$ .

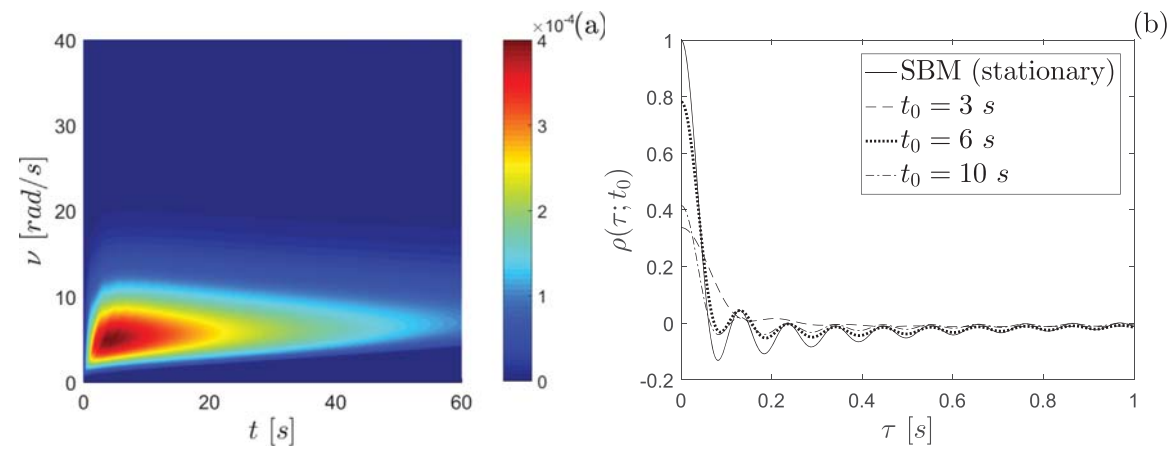


Fig. 11. (a) The power-spectral density function  $g_X(\nu, t|\Theta=[1, 1, 1], \Psi=\widehat{\psi}_{MLE})$  for  $(m, r)=(6.3, 195 \, km)$ , soil type A and far-field seismic regime; (b)  $\rho(\tau, t_0|\Theta=[1, 1, 1], \Psi=\widehat{\psi}_{MLE})$  at fixed times  $t_0 \in \{3, 6, 10\}s$  and the corresponding  $g_{SEM}(\nu)$ .

the sample  $x_i(t_k|\theta_i, \psi_i) = c(t_k)y_i(t_k)$ .

# 4.2. Model comparison

The goal of the ground-motion model is to produce time histories of specified characteristics, such as (m, r), soil type and seismic regime, that are statistically consistent with site records. Since the model for the ground motion-time histories  $X(t; \Theta, \Psi)$  is a stochastic model, a

sample-to-sample comparison is irrelevant. Therefore, statistics of independent models are used for comparison. Simple attenuation relations have been developed for Romania [54] using ground-motion records of major earthquakes in the Vrancea region. One of the equations expresses the peak ground acceleration (PGA) expressed in units of gravity acceleration g in logarithmic scale as a function of moment magnitude m and epicentral distance r:

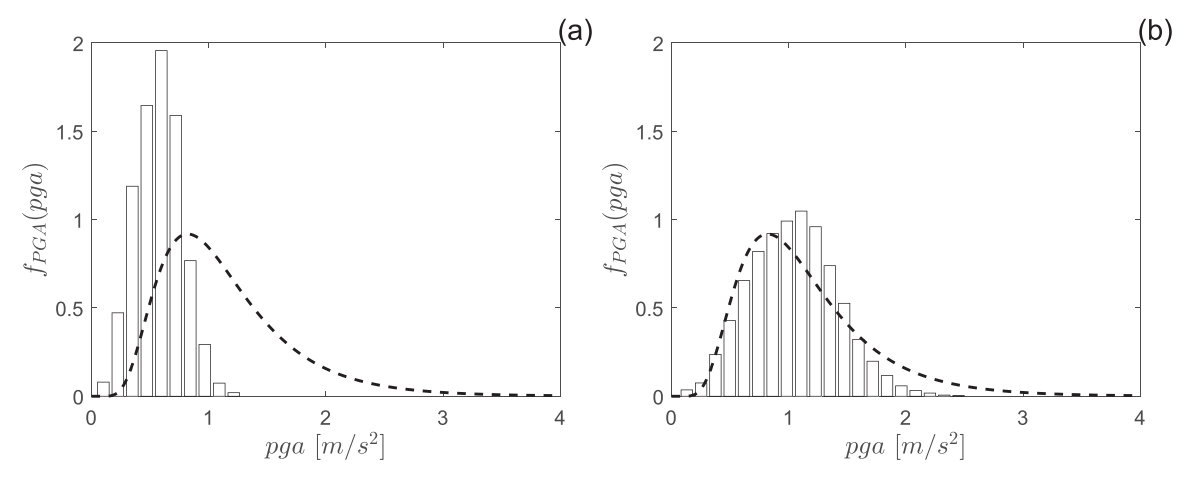


**Fig. 12.** PGA probability density function from the attenuation relation in Eq. (12) vs. histograms of simulated PGA samples of  $X(t; \Theta, \Psi)$ , for  $(m, r) = (6.3, 195 \, km)$ , using (a) Gaussian and (b) non-Gaussian distributions.

$$\ln(PGA) = -9.3922 + 0.9665 m + 0.1149 \ln(r) - 0.004738r, \quad \sigma_{\ln(PGA)}$$
  
= 0.473, (12)

where  $\sigma_{\ln(PGA)}$  is the standard deviation of the  $\ln(PGA)$ . The paper recommends accounting for local soil conditions by scaling  $\ln(PGA)$  values by coefficient S in the range of [0.8, 1.0] for hard rock, [0.7, 0.8] for thin sedimentary layers and [0.65, 0.7] for thick sedimentary layers.

Figs. 12 (a) and (b) compare the histograms of 10, 000 PGA samples of simulated ground-motion records for  $(m, r) = (6.3, 195 \, km)$ , following Gaussian and non-Gaussian distributions, respectively, with the PGA probability-density functions assumed to follow log-normal distributions with parameters calculated by the attenuation law in Eq. (12). These figures show how the inclusion of the kurtosis effect reflected in the simulation of soil conditions results in heavier tails in the distribution of the PGAs, which is more consistent with the distribution assumed in Eq. (12). Note that even though the results are very satisfactory, the comparison in Fig. 12 should be just of a qualitative nature since the results are not expected to match perfectly, given that the two models are conceptually different and are calibrated to different sets of data. The attenuation relation in Eq. (12) is just a regression relation between seismological parameters and PGA observations at various sites. The model developed in this paper is based on prior knowledge given by a global model, the SBM, calibrated solely to records at the site of interest.

Furthermore, an analytical relationship for the probability distribution of the PGA for the model proposed in Eq. (1) can be developed using crossing-rates theory [53] (Section 7.1):

$$F_{PGA}(x) = \exp\left\{-\int_0^{t_f} \eta_X(x, t)dt\right\},\tag{13}$$

where  $\eta_X(x,t)$  are the instantaneous mean crossing rates of the process  $X(t;\Theta,\Psi)$  defined similarly as in Eq. (6), by replacing  $Y(t;\Theta)$  with  $X(t;\Theta,\Psi)$ . Also the second-moment properties of  $X(t;\Theta,\Psi)$ , i.e.  $\sigma(t)$  and  $\dot{\sigma}(t)$ , are calculated using the power-spectral density  $g_X(\nu,t;\Theta,\Psi)$  as:

$$\sigma(t) = \left( \int_{\Theta} \int_{\Psi} \int_{\nu \ge 0} g_X(\nu, t; \theta, \psi) p(\theta, \psi | \widetilde{Z}) d\nu d\psi d\theta \right)^{0.5}, \tag{14}$$

$$\dot{\sigma}(t) = \left( \int_{\Theta} \int_{\Psi} \int_{\nu \ge 0} \nu^2 g_X(\nu, t; \Theta, \Psi) p(\theta, \psi | \widetilde{Z}) d\nu d\psi d\theta \right)^{0.5}, \tag{15}$$

where  $p(\theta, \psi | \widetilde{Z})$  is the posterior distribution on the parameters  $\Theta$  and  $\Psi$ , calculated in Eq. (8). Figs. 13 (a) and (b) show comparisons between the PGA marginal distributions calculated from the attenuation relation in Eq. (12), under the log-normal assumption of the PGA distribution, and the analytical distribution relation calculated in Eq. (13), for

 $(m, r) = (6.3, 195 \, km)$  and  $(m, r) = (7.0, 195 \, km)$ , respectively, events similar to the 1991 and 1977 earthquakes in Romania. It can be concluded that the ground-motion model developed performs well, even at sites with a low number of records, the results being consistent with local empirical results.

#### 5. Conclusions

This paper introduced a novel stochastic earthquake ground-motion model that produces time histories consistent with site records. The model combines in a Bayesian framework the physics from the specificbarrier model, a seismological model calibrated to global data, with site-specific data. The ground-motion time histories are samples of a non-Gaussian, non-stationary stochastic process with frequency content characterized by a one-sided spectral density as a function of seismological parameters, such as moment magnitude, epicentral distance, soil type and seismological regime. The probability law of the stochastic process is governed by stochastic parameters, whose probability distributions are statistically consistent with site data. Analytical relations for the probability distribution of the peak ground acceleration (PGA) are also developed for the updated model. The paper concludes with a step-by-step algorithm that presents both stages of the model, i.e., the calibration to site records and the simulation of samples of ground motions using the distributions of the stochastic parameters.

Among the advantages of the model proposed, the main ones are that it is easy to use; it can be calibrated to a low number of records; and it simulates realistic ground-motion records with minimum computational effort, which allows for the simulation of any number of records. Numerical examples are shown for the proposed model calibrated to the few records available at a nuclear-powerplant site in Romania. The model is validated for this site through a qualitative comparison between the numerical distribution of the PGA obtained from ground-motion simulations and an independent study on the ground-motion prediction equations in the region. The model performs well and it can be used to produce reliable site-specific ground motions for the probabilistic seismic-hazard analyses.

# Acknowledgements

The work presented in this paper has been supported by the Marie Skłodowska-Curie Actions of the European Union's Horizon 2020 Program under the grant agreement 704679 - PARTNER, and by the National Science Foundation under grants CMMI-095714 and CMMI-1639669. This support is gratefully acknowledged.

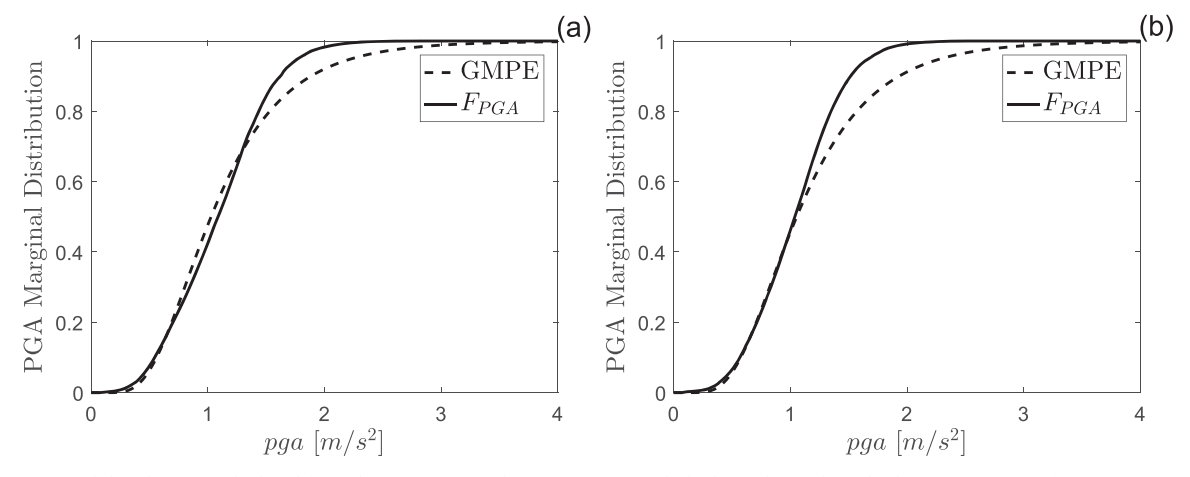


**Fig. 13.** PGA marginal distributions calculated from the attenuation relation in Eq. (12) (dashed) vs. the analytical relation in Eq. (13), for (a)  $(m, r) = (6.3, 195 \, km)$  and (b)  $(m, r) = (7.0, 195 \, km)$ .

#### References

- Katsanos EI, Sextos AG, Manolis GD. Selection of earthquake ground motion records: a state-of-the-art review from a structural engineering perspective. Soil Dyn Earthq Eng 2010;30:158–69.
- [2] Lin T, Haselton C, Baker J. Conditional spectrum-based ground motion selection. Part I: hazard consistency for risk-based assessments. Earthq Eng Struct Dyn 2013;42(12):1847–65.
- [3] Bradley BA, Burks LS, Baker JW. Ground motion selection for simulation-based seismic hazard and structural reliability assessment. Earthq Eng Struct Dyn 2015;44:2322–39.
- [4] Ozer B, Akkar S. A procedure on ground motion selection and scaling for nonlinear response of simple structural systems. Earthq Eng Struct Dyn 2012;41:1693–707.
- [5] Jayaram N, Lin T, Baker J. A computationally efficient ground-motion selection algorithm for matching a target response spectrum mean and variance. Earthq Spectra 2011;27(3):797–815.
- [6] Baker J, Lee C. An improved algorithm for selecting ground motions to match a conditional spectrum. J Earthq Eng 2017:1–16.
- [7] Grigoriu M. To scale or not to scale seismic ground acceleration records. J Eng Mech 2011;137(4):284–93.
- [8] Boore D. SMSIMFortran programs for simulating ground motions from earthquakes: version 2.3a revision of OFR 96-80-a. USGS Open-File Report 2005:00–509.
- [9] Motazedian D, Atkinson GM. Stochastic finite-fault modeling based on a dynamic corner frequency. Bull Seismol Soc Am 2005;95(3):995.
- [10] Boore DM. Comparing stochastic point-source and finite-source ground-motion simulations: SMSIM and EXSIM. Bull Seismol Soc Am 2009;99(6):3202.
- [11] Atkinson GM, Assatourians K, Boore DM, Campbell K, Motazedian D. A guide to differences between stochastic point-source and stochastic finite-fault simulations. Bull Seismol Soc Am 2009;99(6):3192.
- [12] Boore D. Simulation of ground motion using the stochastic method. Pure Appl Geophys 2003;160:635–76.
- [13] Graves RW, Aagaard BT, Hudnut KW. The Shakeout earthquake source and ground motion simulations. Earthq Spectra 2011;27(2):273–91.
- [14] Paolucci R, Evangelista L, Mazzieri I, Schiappapietra E. The 3D numerical simulation of near-source ground motion during the Marsica earthquake, central Italy, 100 years later. Soil Dynamics and Earthquake Engineering, 91, Supplement C. 6ICEGE Earthquake Geotechincal Engineeering; 2016. p. 39–52.
- [15] Ugurhan B, Askan A. Stochastic strong ground motion simulation of the 12 November 1999 Düzce (Turkey) earthquake using a dynamic corner frequency approach. Bull Seismol Soc Am 2010;100(4):1498.
- [16] Ghofrani H, Atkinson GM, Goda K, Assatourians K. Stochastic finite fault simulations of the 2011 Tohoku, Japan, earthquake. Bull Seismol Soc Am 2013;103(2B):1307.
- [17] Goda K, Petrone C, De Risi R, Rossetto T. Stochastic coupled simulation of strong motion and tsunami for the 2011 Tohoku, Japan earthquake. Stoch Environ Res Risk Assess 2016:1–19.
- [18] Seyhan E, Stewart JP, Graves RW. Calibration of a semi-stochastic procedure for simulating high-frequency ground motions. Earthq Spectra 2013;29(4):1495–519.
- [19] Hanks TC, McGuire RK. The character of high-frequency strong ground motion. Bull Seismol Soc Am 1981;71(6):2071.
- [20] Shinozuka M, Deodatis G. Stochastic process models for earthquake ground motion. Probabilistic Eng Mech 1988;3(3):114–23.
- [21] Cacciola P, Deodatis G. A method for generating fully non-stationary and spectrum-compatible ground motion vector processes. Soil Dyn Earthq Eng 2011;31(3):351–60.
- [22] Medel-Vera C, Ji T. A stochastic ground motion accelerogram model for Northwest Europe. Soil Dyn Earthq Eng 2016;82:170–95. [Supplement C].
- [23] Cacciola P. A stochastic approach for generating spectrum compatible fully nonstationary earthquakes. Comput Struct 2010;88(15):889–901.
- [24] Nithin V, Das S, Kaushik H. Wavelet-based simulation of scenario-specific

- nonstationary accelerograms and their GMPE compatibility. Soil Dyn Earthq Eng 2017;99:56–67.
- [25] Rezaeian S, Der Kiureghian A. Simulation of synthetic ground motions for specified earthquake and site characteristics. Earthq Eng Struct Dyn 2010;39(10):1155–80.
- [26] Vlachos C, Papakonstantinou KG, Deodatis G. A multi-modal analytical non-stationary spectral model for characterization and stochastic simulation of earthquake ground motions. Soil Dyn Earthq Eng 2016;80:177–91. [Supplement C].
- [27] Vlachos C, Papakonstantinou KG, Deodatis G. Predictive model for site specific simulation of ground motions based on earthquake scenarios. Earthq Eng Struct Dyn 2017;47(1):195–218.
- [28] Zentner I, Poirion F. Enrichment of seismic ground motions databases using Karhunen-Lòeve expansion. Earthq Eng Struct Dyn 2012.
- [29] Deodatis G. Non-stationary stochastic vector processes: seismic ground motion applications. Probabilistic Eng Mech 1996;11(3):149–67.
- [30] Grigoriu M, Ruiz SE, Rosenblueth E. The Mexico earthquake of september 19, 1985 nonstationary models of seismic ground acceleration. Earthq Spectra 1988:4(3):551–68
- [31] Kiureghian AD, Crempien J. An evolutionary model for earthquake ground motion. Struct Saf 1989:6(2):235–46.
- [32] Conte JP, Peng BF. Fully nonstationary analytical earthquake ground-motion model. J Eng Mech 1997:123(1):15–24.
- [33] Priestley MB. Evolutionary spectra and non-stationary processes. J R Stat Soc Ser B (Methodol) 1965;27(2):204–37.
- [34] Vetter C, Taflanidis AA. Comparison of alternative stochastic ground motion models for seismic risk characterization. Soil Dyn Earthq Eng 2014;58:48–65. [Supplement C].
- [35] Spanos PD, Failla G. Evolutionary spectra estimation using wavelets. J Eng Mech 2004;130(8):952–60.
- [36] Spanos PD, Tezcan J, Tratskas P. Stochastic processes evolutionary spectrum estimation via harmonic wavelets. Comput Methods Appl Mech Eng 2005;194(12):1367–83 [Special Issue on Computational Methods in Stochastic Mechanics and Reliability Analysis].
- [37] Comerford L, Kougioumtzoglou IA, Beer M. Compressive sensing based stochastic process power spectrum estimation subject to missing data. Probabilistic Eng Mech 2016:44:66–76.
- [38] Pousse G, Bonilla L, Cotton F, Margerin L. Nonstationary stochastic simulation of strong ground motion time histories including natural variability: application to the K-net Japanese database. Bull Seismol Soc Am 2006;96(6):2103–17.
- [39] Hwang HH, Huo J-R. Generation of hazard-consistent ground motion. Soil Dyn Earthq Eng 1994;13(6):377–86.
- [40] Trifunac MD. Site conditions and earthquake ground motion a review. Soil Dyn Earthq Eng 2016;90:88–100. [Supplement C].
- [41] Papageorgiou A, Aki K. A specific barrier model for the quantitative description of inhomogeneous faulting and the prediction of strong ground motion. description of the model. Bull Seismol Soc Am 1983;73(3):693–722.
- [42] Halldorsson B, Papageorgiou A. Calibration of the specific barrier model to earth-quake to different tectonic regions. Bull Seismol Soc Am 2005;95(4):1276–300.
- [43] Halldorsson B, Papageorgiou A. Variations of the specific barrier model part I: effect of subevent size distributions. Bull Earthq Eng 2012;10:1299–319.
- [44] Halldorsson B, Papageorgiou A. Variations of the specific barrier model part II: effect of isochron distributions. Bull Earthq Eng 2012;10:1321–37.
- [45] Liu SC. Evolutionary power spectral density of strong-motion earthquakes. Bull Seismol Soc Am 1970;60(3):891.
- [46] Hammond J, White P. The analysis of non-stationary signals using time-frequency methods. J Sound Vib 1996;190(3):419–47.
- [47] Huang NE, Shen Z, Long SR, Wu MC, Shih HH, Zheng Q, Yen N-C, Tung CC, Liu HH. The empirical mode decomposition and the Hilbert spectrum for nonlinear and non-stationary time series analysis. Proceedings of the Royal Society of London A: Mathematical, Physical and Engineering Sciences: 454, 1971; 1998. p. 903–995.
- [48] Radu A, Grigoriu M. A site-specific seismological model for probabilistic seismic-

- hazard assessment. Bull Seismol Soc Am 2014;104(6):3054.
- [49] Ruppert D. What is kurtosis? An influence function approach. Am Stat 1987;41(1):1–5.
- [50] Brys G, Hubert M, Struyf A. Robust measures of tail weight. Comput Stat Data Anal 2006;50:733–59.
- [51] Grigoriu M. Simulation of stationary non-Gaussian translation processes. J Eng Mech 1998;124(2):121–6.
- [52] Grigoriu M. Applied non-Gaussian processes: examples, theory, simulation, linear random vibration, and MATLAB solutions. New Jersey: PTR Prentice Hall; 1995.
  [53] Soong T. Grigoriu M. Random vibration of mechanical and structural systems. New
- [53] Soong T, Grigoriu M. Random vibration of mechanical and structural systems. New Jersey, USA: PTR Prentice - Hall, Inc; 1993.
- [54] Marmureanu G, Androne M, Radulian M, Popescu E, Cioflan CO, Plăcintă AO, et al. Attenuation of the peak ground motion for the special case of Vrancea intermediate-depth earthquakes and seismic hazard assessment at NPP Cernavoda. Acta Geod Et Geophys Hung 2006;41:433–40.
- [55] Luzi L, Puglia R, Russo E, WG5 O. Engineering strong motion database, version 1.0..

- Istituto Nazionale di Geofisica e Vulcanologia, Observatories & Research Facilities for European Seismology; 2016.
- [56] Luzi L, Puglia R, Russo E, D'Amico M, Felicetta C, Pacor F, Lanzano G, Çeken U, Clinton J, Costa G, Duni L, Farzanegan E, Gueguen P, Ionescu C, Kalogeras I, Özener H, Pesaresi D, Sleeman R, Strollo A, Zare M. The engineering strong-motion database: A platform to access pan-European accelerometric data. Seismological Research Letters; 2016.
- [57] Lungu D, Arion C, Aldea A, Vacareanu R. Evolutionary power spectral density of strong-motion earthquakes. In: Proceedings of the 13th world conference on earthquake engineering: Vancouver, Canada, no. 1796; 2004.
- [58] Clrau E-A. Methodological aspects regarding the assessment of soil conditions with applications in seismic microzonation studies. Bul Stiint UTCB 2012;4:27–35.
- [59] Bucur C, Olteanu M, Pavelescu M. Radionuclide diffusion in geological media. Rom J Phys 2006;51(3–4):469–78.
- [60] Grigoriu M. Stochastic systems. Uncertainty quantification and propagation. London, UK: Springer-Verlag Ltd; 2012.